



Reverse Monte Carlo modeling for catalyst nanoparticles in polymer electrolyte fuel cells by high-energy X-ray diffraction

Yuki Mizuno¹, Hirokazu Tsuji^{1,2}, Satoshi Hiroi^{1,3} , Tomoya Uruga¹ , Takuma Kaneko¹, Kengo Nakada⁴, Koji Ohara^{1,3} , Hideto Imai^{5,6}, Yoshiharu Uchimoto⁵ , Yoshiharu Sakurai¹

Keywords:

Reverse Monte Carlo, nanoparticle, catalysts

Citation:

Mizuno, Y.; Tsuji, H.; Hiroi, S.; Uruga, T.; Kaneko, T.; Nakada, K.; Ohara, K.; Imai, H.; Uchimoto, Y.; Sakurai, Y. Reverse Monte Carlo modeling for catalyst nanoparticles in polymer electrolyte fuel cells by high-energy X-ray diffraction. *Microstructures* 2026, 6, 2026045. <https://dx.doi.org/10.20517/microstructures.2025.72>

Received: 25 May 2025

First Decision: 22 Jul 2025

Revised: 19 Aug 2025

Accepted: 2 Sep 2025

Published: 16 Apr 2026

Academic Editor:

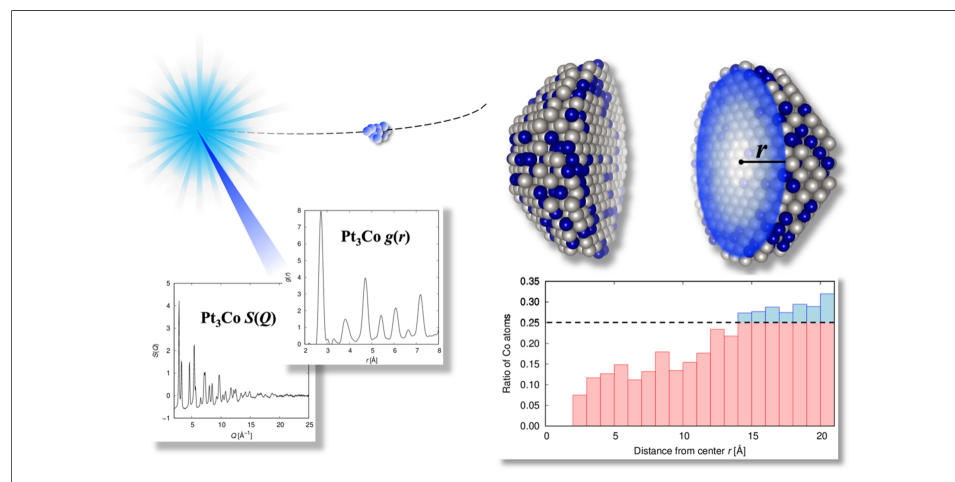
Yida Deng

Copy Editor:

Fangling Lan

Production Editor:

Fangling Lan



Abstract

To elucidate the correlation between the catalytic properties of metal nanoparticles used in polymer electrolyte fuel cells and the atomic arrangements of such nanoparticles, high-energy X-ray diffraction measurements were conducted. Using the measured data as a reference, Reverse Monte Carlo was performed on isolated finite-size spherical cluster models to visualize the atomic arrangements of Pt and Pt₃Co nanoparticles. In the Pt₃Co nanoparticles, the local composition of the nanoparticle center and the surface region differed. The tendency of Co atoms to be located closer to the surface rather than the center was confirmed. Furthermore, the atomic arrangements in the center of the Pt and Pt₃Co nanoparticles were more disordered than those in the surface region. Thus, we clarified the difference in the distribution of atoms in the center and surface regions by creating a three-dimensional model of the atomic arrangement of the nanoparticles. The

¹Japan Synchrotron Radiation Research Institute, 1-1-1, Kouto, Sayo-cho, Sayo-gun, Hyogo 679-5198, Japan.

²Sumitomo Electric Industries, Ltd., Osaka 541-0041, Japan.

³Faculty of Materials for Energy, Shimane University, 1060, Nishikawatsu-cho, Matsue, Shimane 690-8504, Japan.

⁴Co-Creation Institute for Advanced Materials, Shimane University, Matsue, Shimane 690-8504, Japan.

⁵Graduate School of Human and Environmental Studies, Kyoto University, Yoshida-nihonmatsu-cho, Sakyo-ku, Kyoto 606-8501, Japan.

⁶Fuel Cell Cutting-Edge Research Center Technology Research Association, Kofu 400-1507, Japan.

Correspondence to: Asst. Prof. Satoshi Hiroi, Japan Synchrotron Radiation Research Institute, 1-1-1, Kouto, Sayo-cho, Sayo-gun, Hyogo 679-5198, Japan; Faculty of Materials for Energy, Shimane University, 1060, Nishikawatsu-cho, Matsue, Shimane 690-8504, Japan. E-mail: s_hiroi@mat.shimane-u.ac.jp; Asst. Prof. Yoshiharu Sakurai, Japan Synchrotron Radiation Research Institute, 1-1-1, Kouto, Sayo-cho, Sayo-gun, Hyogo 679-5198, Japan. E-mail: sakurai@spring8.or.jp

visualized structural model can contribute to the development and performance enhancement of nanoparticle catalysts.

INTRODUCTION

In the bid to achieve carbon neutrality by 2050, fuel cells (FCs), which convert the energy of water production from hydrogen and oxygen in the air into electricity, have been touted as potential power generation devices for hydrogen utilization^[1]. FC vehicles (FCVs) have recently been commercialized, and polymer electrolyte FCs (PEFCs) have begun to be used as a power source for FCVs. PEFCs present significant advantages, as they exhibit a high power generation efficiency and do not produce carbon dioxide^[2]. However, the commercialization of Pt nanoparticles, a precious metal, as catalysts for the hydrogen and oxygen electrodes of PEFCs has been slow because of the high price of PEFCs for high-power FCVs, which require a large amount of catalysts. In particular, the reduction reaction at the oxygen electrode is slower than the oxidation reaction at the hydrogen electrode^[3,4]. Furthermore, the large amount of Pt used in the oxygen electrode hinders a reduction in PEFC costs. Pt catalysts with superior performance, i.e., high oxygen reduction reaction activity and durability, are required to reduce the amount of Pt needed.

The nanoparticles used as catalysts in PEFCs are crystallites (diameters of approximately 1-5 nm) and are characterized by a large proportion of interfaces. Thus, the structure and properties of the nanoparticles differ from those of the bulk metal. The number of atoms in the surface layer of such small metal nanoparticles is comparable to the number of atoms within the nanoparticles. Thus, it is important to investigate the three-dimensional (3D) atomic arrangement of the entire nanoparticle to understand the relationship between its atomic structure and catalytic properties.

To date, pair distribution function (PDF) analysis based on high-energy X-ray diffraction (HEXRD) has been employed to examine the 3D atomic arrangements of metal nanoparticles that deviate from the corresponding bulk crystal structures^[5,6]. Furthermore, Reverse Monte Carlo (RMC) modeling^[7,8] based on HEXRD data suggests that the atomic-scale structures of metal nanoparticles, such as Pt, Pd, Rh, and Ru, exhibit clear structural disorder^[9-11]. Conventional RMC modeling is not suitable for modeling the atomic structure of nanoparticles because it assumes a homogeneous bulk metal. This is because, as the particle size decreases, the ratio of surface to core atoms becomes significant. In addition to such structural approaches, density functional theory (DFT) calculations have also been shown to provide valuable insights into catalytic mechanisms^[12], highlighting the complementarity of experimental and theoretical analyses.

In 2013, Gereben and Petkov developed an RMC approach with nonperiodic boundary conditions (NP-RMC). Since NP-RMC enables the modeling of samples confined to finite sizes such as nanoparticles, it facilitates the analysis of structural differences between the core and surface. In particular, when the target material functions as a catalyst, the reaction sites are located on the surface; therefore, understanding the structural characteristics of the surface is crucial. Here, the 3D structural modeling of Pt and Pt₃Co nanoparticles was performed via the RMC simulations of isolated finite-size spherical cluster models without periodic boundary conditions using HEXRD data to clarify the atomic arrangements associated with catalytic properties.

MATERIALS AND METHODS

Sample preparation

A carbon-supported Pt catalyst (TEC10V30E, Tanaka Kikinzoku Kogyo) and a carbon-supported PtCo catalyst (TEC36F52, Tanaka Kikinzoku Kogyo) were used as samples. Although they are commercial products, it is important to investigate their structures, as they can serve as standard samples for evaluating

various catalyst samples in the future. The powder samples were reduced in a reaction vessel filled with high-purity hydrogen gas at room temperature for 30 min. The vessel was opened in a glove box under an Ar atmosphere and the samples were loaded into a quartz glass capillary (diameter = 1 mm).

High-energy X-ray diffraction measurements

HEXRD measurements were performed at the BL04B2 beamline^[13,14] in SPring-8, Hyogo, Japan, to reveal the local atomic configuration of the synthesized nanoparticle catalysts. The incident X-ray beam (energy = 61.4 keV) was monochromated by the Si 220 reflection of a bent monochromator installed in the beamline. The scattered X-ray photons from the sample powders were counted using four CdTe detectors (X-123CdTe, Amptek) and three highly pure Ge solid-state detectors (GL0515, Canberra Industries) installed at 8° intervals. The measurements were performed within a 2θ range of 0.3°–57°; thus, the maximum momentum transfer Q_{\max} was approximately 29.6 Å⁻¹. The coherent X-ray scattering intensity $I_{\text{coh}}(Q)$ was obtained by subtracting the X-ray absorption, Compton scattering, and contribution of the quartz capillary from the raw X-ray scattering intensity. The structure factor $S(Q)$ was obtained by normalizing the $I_{\text{coh}}(Q)$ ^[15]:

$$S(Q) = 1 + \frac{I_{\text{coh}}(Q) - \sum_i c_i |f_i(Q)|^2}{|\sum_i c_i f_i(Q)|^2},$$

where c_i and $f_i(Q)$ are the atomic concentration and X-ray atomic scattering factor of the i -th element in the material, respectively. The PDF, $g(r)$, was calculated using the Fourier transform of $S(Q)$:

$$g(r) = 1 + \frac{1}{2\pi^2 r \rho} \int_{Q_{\min}}^{Q_{\max}} Q \{S(Q) - 1\} \sin(Qr) dQ,$$

where ρ is the atomic number density, and r is the radial distance. The upper limit of the integral was Q_{\max} , which was determined by the experimental conditions. The sequential analyses were executed with the original software for the BL04B2 beamline.

Reverse Monte Carlo modeling

The atomic configuration of the nanoparticle catalysts was constructed via RMC modeling^[7,8] with nonperiodic boundary conditions (NP-RMC)^[9,16] using the obtained $S(Q)$ values. Table 1 summarizes the structural information of the initial models of the Pt nanoparticles in TEC10V30E (average particle size of 3 nm, as observed via TEM) and Pt₃Co nanoparticles in TEC36F52 (average particle size of 4 nm, as observed via TEM). The initial model of the Pt nanoparticle was a sphere (diameter = 30 Å) cut from face-centered cubic (fcc)-type bulk Pt with the space group $Fm-3m$ and a lattice constant of 3.902 Å, as determined by XRD analysis. The initial model of the Pt₃Co nanoparticle was a sphere (diameter = 40 Å) cut from fcc-type bulk Pt₃Co with the space group $Fm-3m$ and a lattice constant of 3.859 Å, as determined by XRD analysis. Figure 1 shows a snapshot of the initial atomic configurations. During the NP-RMC calculations, the nearest neighbor cut-off distances were set to 2.4 Å for all the atomic pairs, Pt-Pt, Co-Co, and Pt-Co. The swapping of Pt and Co atoms is allowed for Pt₃Co nanoparticles. Two kinds of movements (atomic translational movement and the exchange of different atomic pairs) enable the generation of configurations for the next MC step. The trial ratio of exchanging positions to all trials to generate configurations was set to 30%. Furthermore, to restrict the translational movement of the atoms to the area around the lattice points, fittings were simultaneously performed for the low- r region of the $g(r)$ and $S(Q)$. Atoms constantly oscillate around their equilibrium position, leading to the broadening of the Bragg and $g(r)$ peaks in crystals. Thus, the effect of atomic oscillations is incorporated into the fitting to the $g(r)$ by convolving the Gaussian function with the variance $\sigma = 0.04$ Å.

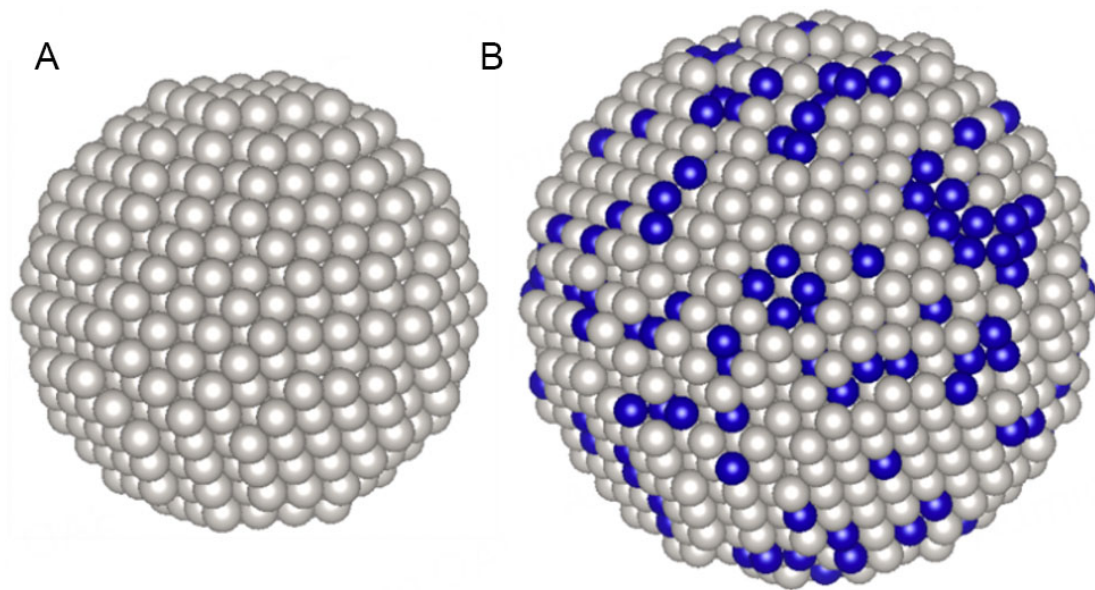


Figure 1. Snapshot of the initial atomic configurations of a Pt nanoparticle in TEC10V30E (A) and a Pt₃Co nanoparticle in TEC36F52 (B). White and blue spheres represent Pt and Co atoms, respectively.

Table 1. Structural information of the initial models of the Pt and Pt₃Co nanoparticles

Sample	TEC10V30E	TEC36F52
Composition	Pt	Pt ₃ Co
Lattice constant (fcc)	3.902 Å	3.859 Å
Number of atoms	959 (Pt: 959)	2315 (Pt: 1744, Co: 571)
Simulation diameter	30 Å	40 Å

The R_w value used usually in crystallography to characterize the goodness of the fit is calculated for the $g(r)$ and $S(Q)$ data series, according to the formula:

$$R_w = \left\{ \frac{\sum w_i (\chi_i^E - \chi_i^C)^2}{\sum w_i (\chi_i^E)^2} \right\}^{\frac{1}{2}}$$

where χ_i^E and χ_i^C are the experimental and calculation data, respectively. w_i is the weighting factor reflecting the statistical quality of the individual data points^[11].

In this study, we focus on nanoparticles in a static environment similar to a vacuum or inert conditions. However, during actual PEMFC operation, catalysts are exposed to a dynamic environment involving oxidation, hydration, and potential structural rearrangements. Although reproducing such dynamic environments using RMC is challenging, it is possible to discuss structural changes by performing similar experiments and modeling on nanoparticles after exposure to these dynamic conditions.

RESULTS AND DISCUSSION

Figure 2 shows the $S(Q)$ and $g(r)$ obtained via HEXRD measurements. A broadened Bragg peak profile corresponding to the nano-order crystallite size was confirmed for the $S(Q)$ of both samples, and these profiles corresponded to the fcc crystal structure. Similarly, the $g(r)$ exhibited peaks corresponding to the

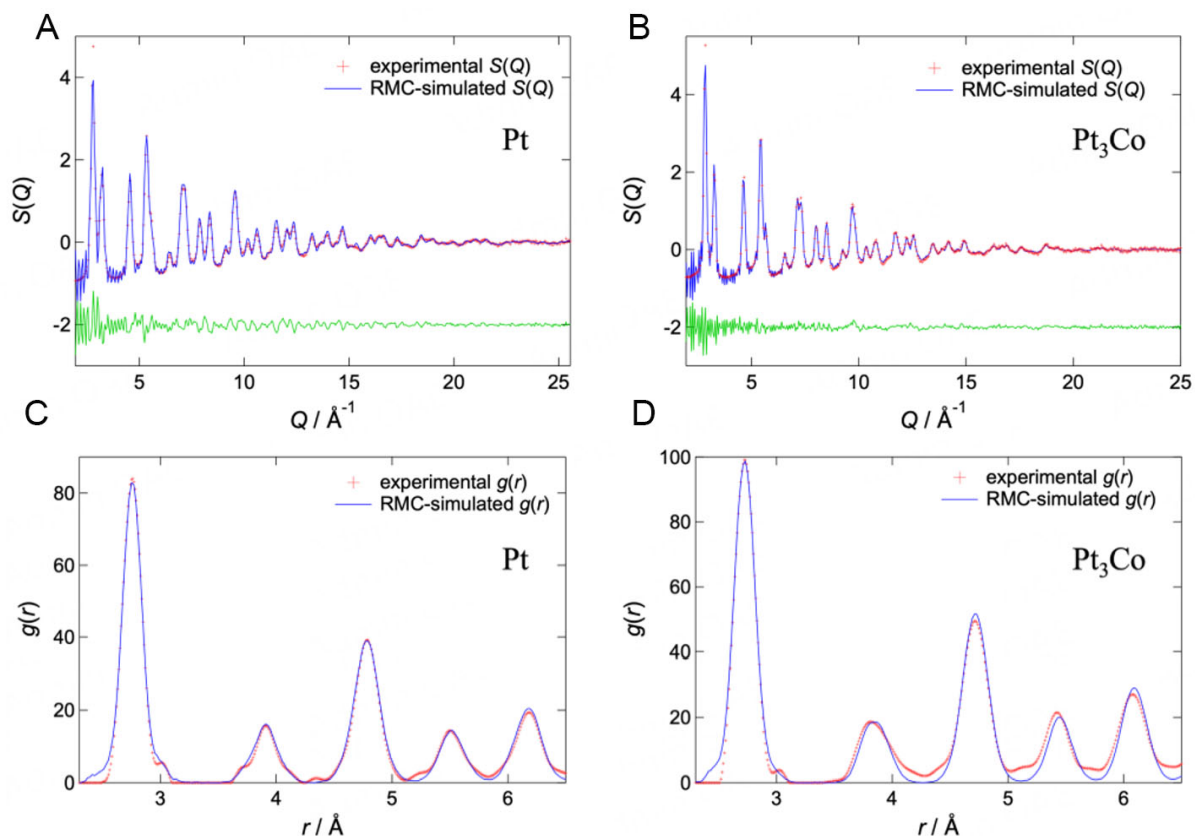


Figure 2. Results of HEXRD measurements and NP-RMC fittings. Structure factors $S(Q)$ of the Pt (A) and Pt_3Co (B) nanoparticles, as well as the pair distribution functions $g(r)$ of the Pt (C) and Pt_3Co (D) nanoparticles. The red, blue, and green marks represent the experimental data, RMC-simulated data, and the differences between both, respectively.

interatomic distances of the fcc crystal structure. These peaks were separated from each other because of a few disordered atomic configurations, such as the amorphous phase in the nanoparticles.

Figure 2 shows the $S(Q)$ and $g(r)$ of the final atomic configurations obtained via NP-RMC modeling. For both samples, the goodness-of-fit indicator R_w for fitting to the $S(Q)$ via NP-RMC modeling reached 22%–23%. Considering that the experimental $S(Q)$ was consistent with the calculated $S(Q)$, it is considered that the obtained atomic arrangement of the nanoparticles had been well characterized. Figure 3A shows the ratio of Co atoms as a function of the distance from the center of the nanoparticles to visualize the spatial concentration distribution of the Pt_3Co nanoparticles. This shows that Co atoms tend to be located on the surface region of Pt_3Co nanoparticles. The snapshot of the atomic arrangement model obtained via NP-RMC modeling [Figure 3B] visually confirms the presence of many Co atoms on the nanoparticle surface. Through an analysis of the spatial concentration distribution in the nanoparticles, we can determine the composition of the surface region that contributes to catalytic reactions. Thus, atomic arrangement modeling via NP-RMC can provide insights into the prediction of catalytic activity and durability from the viewpoint of nanoparticle structure.

The neighboring distance distribution for the nanoparticle crystals was analyzed to characterize the disorder of the atomic configuration. Thus, NP-RMC calculations were performed 10 times for each nanoparticle under the same calculation conditions, and the neighboring distance distributions of the results were added to improve the statistical accuracy. Figure 4 shows the neighboring distance distribution for the Pt and Pt_3Co nanoparticles based on the atomic configuration. For the Pt nanoparticles, the surface and internal atoms

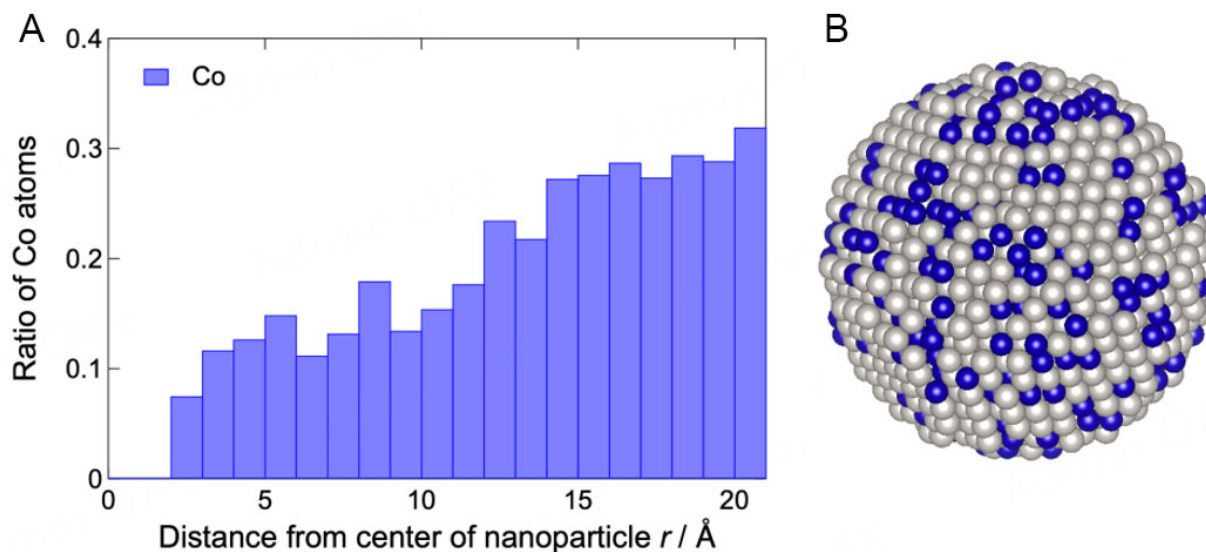


Figure 3. Ratio of Co atoms as a function of the distance from the center (A) of the nanoparticles. Snapshot (B) of the final atomic configuration of the Pt_3Co nanoparticles. White and blue spheres represent Pt and Co atoms, respectively.

Table 2. Neighboring distance distribution parameters for the Pt and Pt_3Co nanoparticles

Pairs (Pt nanoparticles)	Average distance	FWHM
Pt-Pt (core)	2.75 Å	0.18 Å
Pt-Pt (surface)	2.75 Å	0.15 Å
Pairs (Pt_3Co nanoparticles)	Average distance	FWHM
Pt-Pt (core)	2.73 Å	0.19 Å
Pt-Co (core)	2.72 Å	0.26 Å
Co-Co (core)	2.73 Å	0.20 Å
Pt-Pt (surface)	2.73 Å	0.16 Å
Pt-Co (surface)	2.72 Å	0.22 Å
Co-Co (surface)	2.73 Å	0.17 Å

were divided at 13 Å, and their distributions are shown in Figure 4. We divided the atoms into two categories based on the distance from the surface to the second atomic layer (the boundary where the coordination number becomes 12). For Pt_3Co nanoparticles, the same was observed at 17 Å. Table 2 lists the average distances and full width at half maximum (FWHM) values of the distributions. Here, the neighboring atoms indicate 12 coordinating atoms in the fcc crystal structure. The average distance of the neighboring distance distribution of the Pt nanoparticle was the same for the core and surface regions. Contrarily, the FWHM in the core region was larger than that in the surface region. A similar trend was observed for the distribution of the Pt_3Co nanoparticles. For both Pt and Pt_3Co nanoparticles, the structural disorder was observed to be smaller on the surface than in the core. Comparing the distributions of the Pt and Pt_3Co nanoparticles, the FWHMs of the distribution of Pt_3Co nanoparticles exceeded those of Pt nanoparticles both in the core and on the surface. Thus, the Pt_3Co nanoparticles in TEC36F52, which contain Co atoms, were observed to exhibit a slightly more disordered crystal structure than the Pt nanoparticles in TEC10V30E.

An understanding of the atomic arrangement of the surface region will prove useful in the prediction of catalytic properties since catalytic reactions occur on the surface of nanoparticles. This will facilitate an evaluation of the catalytic activity and durability of nanoparticles using new variables, such as the

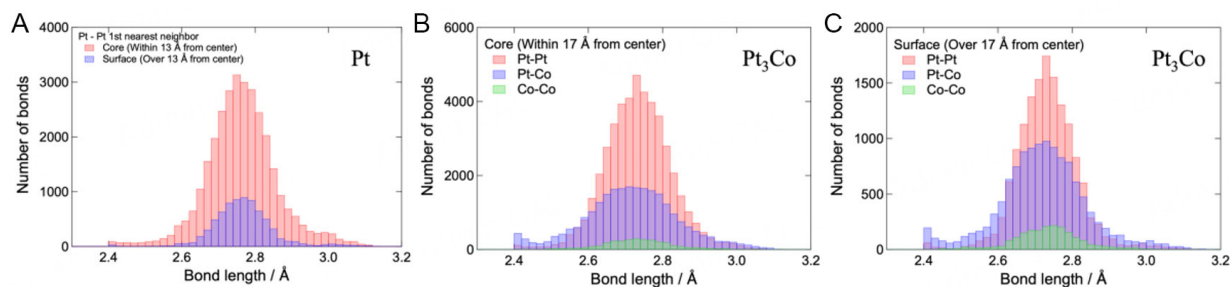


Figure 4. Neighboring distance distribution of atoms in the Pt nanoparticles (A) and of internal (B) and surface (C) atoms in the Pt₃Co nanoparticles. For the Pt nanoparticles, the red and blue bars represent the distributions of internal and surface atoms, respectively. Oppositely, for the Pt₃Co nanoparticles, the red, blue, and green bars represent the Pt-Pt, Pt-Co, and Co-Co correlation distributions, respectively.

composition of the surface region, disorder in the crystal lattice, and particle size, which is related to the surface area. These variables can then be used to elucidate the structural features that strongly contribute to the catalytic properties. We expect that the development of nanoparticle catalysts using HEXRD and NP-RMC will be dramatically accelerated by establishing a technique for evaluating catalytic properties from a microscopic viewpoint.

CONCLUSIONS

Here, Pt and Pt₃Co nanoparticles were subjected to HEXRD measurements to clarify the correlation between the local atomic configuration and catalytic activity. Furthermore, 3D atomic configuration models were successfully constructed via NP-RMC modeling based on the experimental $S(Q)$ and $g(r)$. From the structural model, features such as spatial concentration and atomic arrangement disorder were extracted. In the Pt₃Co nanoparticles, the dependence of Pt and Co concentrations on the distance from the center was confirmed. Fewer Co atoms were observed in the center, and more Co atoms were observed near the surface. NP-RMC modeling, which permits Pt and Co swapping, confirmed the difference between the core and surface Co distributions. The distributions of the distance between neighboring atoms were derived from the obtained models. For both Pt and Pt₃Co nanoparticles, the distributions were slightly wider in the core region than in the surface region, indicating that the atomic arrangement was more disordered in the core region than in the surface region. Furthermore, the width of the distribution of the Pt₃Co nanoparticles exceeded that of the Pt nanoparticles, indicating that the disorder in the atomic arrangement of the Pt₃Co nanoparticles was due to the presence of Co atoms.

Nanoparticles are promising as catalysts because of their large surface area for chemical reactions. Here, the atomic distribution of the surface region and the degree of disorder in the atomic arrangement were successfully determined by modeling the atomic arrangement of nanoparticles via NP-RMC. This study provides insights into the development of catalytic properties based on an understanding of the atomic configuration of nanoparticles.

DECLARATIONS

Acknowledgments

Synchrotron radiation experiments were performed with the approval of the Japan Synchrotron Radiation Research Institute (JASRI) (Proposal Nos. 2021B1016, 2022A1014, and 2022B1006).

Authors' contributions

Study conception and design, data analysis, commented on the first version of the manuscript: Mizuno, Y.; Tsuji, H.; Hiroi, S.; Uruga, T.; Kaneko, T.; Nakada, K.; Ohara, K.; Imai, H.; Uchimoto, Y.; Sakurai, Y.

Material preparation: Imai, H.

Data collection: Mizuno, Y.; Tsuji, H.; Hiroi, S.; Ohara, K.

The first draft of the manuscript was written: Mizuno, Y.; Hiroi, S.; Ohara, K.
All authors read and approved the final manuscript.

Availability of data and materials

Data are available from the corresponding authors upon reasonable request.

AI and AI-assisted tools statement

Not applicable.

Financial support and sponsorship

This work is based on results obtained from an FC-Platform project (P20003) commissioned by the New Energy and Industrial Technology Development Organization (NEDO).

Conflicts of interest

All authors declared that there are no conflicts of interest.

Ethical approval and consent to participate

Not applicable.

Consent for publication

Not applicable.

Copyright

© The Author(s) 2026.

REFERENCES

1. Steele, B. C. H.; Heinzel, A. Materials for fuel-cell technologies. *Nature* **2001**, *414*, 345-52. DOI
2. Wang, Y.; Diaz, D. F. R.; Chen, K. S.; Wang, Z.; Adroher, X. C. Materials, technological status, and fundamentals of PEM fuel cells - A review. *Mater. Today* **2020**, *32*, 178-203. DOI
3. Debe, M. K. Electrocatalyst approaches and challenges for automotive fuel cells. *Nature* **2012**, *486*, 43-51. DOI PubMed
4. Strmcnik, D.; Escudero-Escribano, M.; Kodama, K.; Stamenkovic, V. R.; Cuesta, A.; Marković, N. M. Enhanced electrocatalysis of the oxygen reduction reaction based on patterning of platinum surfaces with cyanide. *Nat. Chem.* **2010**, *2*, 880-5. DOI PubMed
5. Petkov, V. Nanostructure by high-energy X-ray diffraction. *Mater. Today* **2008**, *11*, 28-38. DOI
6. Petkov, V.; Bedford, N.; Knecht, M. R.; et al. Periodicity and atomic ordering in nanosized particles of crystals. *J. Phys. Chem. C* **2008**, *112*, 8907-11. DOI
7. McGreevy, R. L.; Pusztai, L. Reverse Monte Carlo simulation: a new technique for the determination of disordered structures. *Mol. Simul.* **1988**, *1*, 359-67. DOI
8. McGreevy, R. L. Reverse Monte Carlo modelling. *J. Phys. Condens. Matter* **2001**, *13*, R877-913. DOI
9. Gereben, O.; Petkov, V. Reverse Monte Carlo study of spherical sample under non-periodic boundary conditions: the structure of Ru nanoparticles based on x-ray diffraction data. *J. Phys. Condens. Matter* **2013**, *25*, 454211. DOI
10. Kumara, L. S.; Sakata, O.; Kohara, S.; et al. Origin of the catalytic activity of face-centered-cubic ruthenium nanoparticles determined from an atomic-scale structure. *Phys. Chem. Chem. Phys.* **2016**, *18*, 30622-9. DOI
11. Harada, M.; Ikegami, R.; Kumara, L. S. R.; Kohara, S.; Sakata, O. Reverse Monte Carlo modeling for local structures of noble metal nanoparticles using high-energy XRD and EXAFS. *RSC Adv.* **2019**, *9*, 29511-21. DOI PubMed PMC
12. Wang, J.; Zhang, J.; Zhang, Y.; et al. Atom-level tandem catalysis in lithium metal batteries. *Adv. Mater.* **2024**, *36*, e2402792. DOI
13. Isshiki, M.; Ohishi, Y.; Goto, S.; Takeshita, K.; Ishikawa, T. High-energy X-ray diffraction beamline: BL04B2 at SPring-8. *Nucl. Instrum. Methods Phys. Res. A* **2001**, *467-8*, 663-6. DOI
14. Ohara, K.; Onodera, Y.; Murakami, M.; Kohara, S. Structure of disordered materials under ambient to extreme conditions revealed by synchrotron X-ray diffraction techniques at SPring-8-recent instrumentation and synergic collaboration with modelling and topological analyses. *J. Phys. Condens. Matter* **2021**, *33*, 383001. DOI PubMed
15. Billinge, S. J.; Kanatzidis, M. G. Beyond crystallography: the study of disorder, nanocrystallinity and crystallographically challenged materials with pair distribution functions. *Chem. Commun.* **2004**, *7*, 749-60. DOI
16. Gereben, O.; Pusztai, L. RMC_POT: a computer code for reverse Monte Carlo modeling the structure of disordered systems containing molecules of arbitrary complexity. *J. Comput. Chem.* **2012**, *33*, 2285-91. DOI

Disclaimer/Publisher's Note: All statements, opinions, and data contained in this publication are solely those of the individual author(s) and contributor(s) and do not necessarily reflect those of OAE and/or the editor(s). OAE and/or the editor(s) disclaim any responsibility for harm to persons or property resulting from the use of any ideas, methods, instructions, or products mentioned in the content.



© The Author(s) 2026. Open Access This article is licensed under a Creative Commons Attribution 4.0 International License (<https://creativecommons.org/licenses/by/4.0/>), which permits unrestricted use, sharing, adaptation, distribution and reproduction in any medium or format, for any purpose, even commercially, as long as you give appropriate credit to the original author(s) and the source, provide a link to the Creative Commons license, and indicate if changes were made.